

Supporting Information

Highly Efficient Red Thermally Activated Delayed Fluorescence Emitters by Manipulating Molecular Horizontal Orientation

Changjiang Zhou,^{a,b,†} Chen Cao,^{c,†} Dezhi Yang,^d Xiaosong Cao,^{*,a} He Liu,^a Dongge Ma,^d Chun-Sing Lee,^{*,c} Chuluo Yang^{*,a}

^a Shenzhen Key Laboratory of Polymer Science and Technology, College of Materials Science and Engineering, Shenzhen University, Shenzhen 518060, P. R. China

^b College of Physics and Optoelectronic Engineering, Shenzhen University, Shenzhen 518060, P. R. China

^c Center of Super-Diamond and Advanced Films (COSDAF) and Department of Chemistry, City University of Hong Kong, Kowloon, Hong Kong SAR 999077, P. R. China

^d Center for Aggregation-Induced Emission, Institute of Polymer Optoelectronic Materials and Devices, Guangdong Provincial Key Laboratory of Luminescence from Molecular Aggregates, State Key Laboratory of Luminescent Materials and Devices, South China University of Technology, Guangzhou 510640, People's Republic of China

Contents

S-I Characterization and Measurements

S-II Synthesis

S- III Figures

S-I Characterization and Measurements

General information: The ^1H NMR spectra were recorded on AVANCE 500 spectrometers at 298 K by utilizing CDCl_3 as solvents and tetramethylsilane (TMS) as a standard. High-resolution mass spectrometry (HRMS) was performed using FAB^+ ionization on a JEOL MS Route mass spectrometer. Thermal gravimetric analysis (TGA) was undertaken on a PerkinElmer thermal analysis system at a heating rate of $10\text{ }^\circ\text{C min}^{-1}$ and a nitrogen flow rate of 80 mL min^{-1} . The temperature of degradation (T_d) was correlated to a 5% weight loss.

Photophysical measurements: The UV-vis absorption spectra were obtained on a Shimadzu UV-2600 spectrophotometer (Shimadzu, Japan) at room temperature. Room-temperature photoluminescence spectra and phosphorescence spectra were measured on a Hitachi F-7100 fluorescence spectrophotometer. The lifetimes of delayed fluorescence were obtained by PicoQuant Fluotime300 with an EPL-375 optical laser. The solid state absolute PLQYs were measured on a Quantaaurus QY measurement system (C9920-02, Hamamatsu Photonics) equipped with a calibrated integrating sphere in the host of CBP (7 wt%) and all the samples were excited at 350 nm. During the PLQY measurements, the integrating sphere was purged with pure and dry argon to maintain an inert environment.

Quantum chemical calculations: All the density functional theory (DFT) calculations were carried out using Gaussian 09 (version D.01) package on a PowerLeader cluster. The ground-state and excited state (S_1) geometries were fully optimized using DFT with B3LYP-D3(BJ) (empirical dispersion = gd3) hybrid functional at the basis set level of def2-SVP. The excited-state properties were obtained by time-dependent density functional theory (TD-DFT) at the basis set level of PBE0/def2-SVP. Based on the optimized S_1 state geometries and vibrational normal modes, the nuclear ensemble approach was performed with the Newton-X program. A total of 300 nuclear configurations were sampled according to the finite-temperature uncorrelated Wigner distribution for room temperature (300 K). TDDFT calculations for $S_1 \rightarrow S_0$ transitions were then performed at the same level to collect the TDMs, oscillator strength, and transition energies of all the configurations. Arithmetic means of the f and x , y and z components of TDM were then calculated to describe the radiative transition in the dynamic disorder system. The direction of the calculated transition dipole moments (TDMs) and oscillator strengths (f 's) were extracted from the simulated S_1 structures (Figure1). S_1 state geometries are optimized at PBE0/def-SVP level with Grimme's D3BJ empirical dispersion correction using TDDFT method.

Determination of the emitting dipole orientation of an emitting layer: To determine emitting dipole orientation of an emitting film, angle-resolved and polarization-resolved PL measurements were performed. The sample consisted of a fused silica substrate with the 60-nm-thick CBP host film doped with emitters. The sample was

attached to a fused silica half-cylinder prism by index matching liquid. The excitation of the samples was performed with the 350-nm line of the continuous-wave He:Cd laser with a fixed excitation angle of 45°. The emission angle was changed by use of an automatic rotation stage. The spectra were resolved by utilization of a *p*-polarizing filter and measured by a fiber optical spectrometer. The angle-dependent *p*-polarized emission intensity at the peak wavelength of the PL spectrum of the emitting layer was detected. The emitting dipole orientation ($\Theta//$) was then determined by least-square fitting of the measured angle-dependent *p*-polarized emission intensity with calculated results.

Electrochemical characterization: Cyclic voltammetry (CV) was performed with a BAS 100W Bioanalytical Systems, using a glass carbon disk ($\Phi = 3$ mm) as the working electrode, a platinum wire as the auxiliary electrode with a porous ceramic wick, Ag/Ag⁺ as the reference electrode, standardized for the redox couple ferricinium/ferrocene. All solutions were purged with a nitrogen stream for 10 min before measurement. The procedure was performed at room temperature and a nitrogen atmosphere was maintained over the solution during measurements.

Device fabrication and performances: ITO-coated glass with a sheet resistance of 15 Ω square⁻¹ was used as the substrate. Before device fabrication, the ITO glass substrates were cleaned by deionized water, isopropyl alcohol, acetone and chloroform with ultrasonic cleaner. After treated with UV-zone for 30 min, ITO glasses were transferred to a vacuum deposition system with the base pressure lower than 5 x 10⁻⁴ Pa for organic and metal deposition. The devices were fabricated by evaporating organic layers with an evaporation rate of 0.5-0.8 Å s⁻¹. The cathode was completed through thermal deposition of LiF at a deposition rate of 0.1 Å s⁻¹, and then capped with Al through thermal deposition at a deposition rate of 3-5 Å s⁻¹. Electroluminescence spectra and the corresponding luminance were recorded using PMA-12 photonic multichannel analyzer (Hamamatsu), and the current density-voltage-luminance characteristics were measured by computer controlled Keithley 237 power source (Tektronix) under ambient atmosphere.

Calculation of the rate constants: The rate constants of excited state dynamics were calculated through following equations:

$$\Phi = \Phi_{PF} + \Phi_{TADF} \quad (4)$$

$$k_r = \Phi_{PF}/\tau_{PF} \quad (5)$$

$$\Phi = k_r/(k_r + k_{nr}) \quad (6)$$

$$\Phi_{PF} = k_r/(k_r + k_{isc} + k_{nr}) \quad (7)$$

$$k_{risc} = k_p k_d \Phi_{TADF} / k_{isc} \Phi_{PF} \quad (8)$$

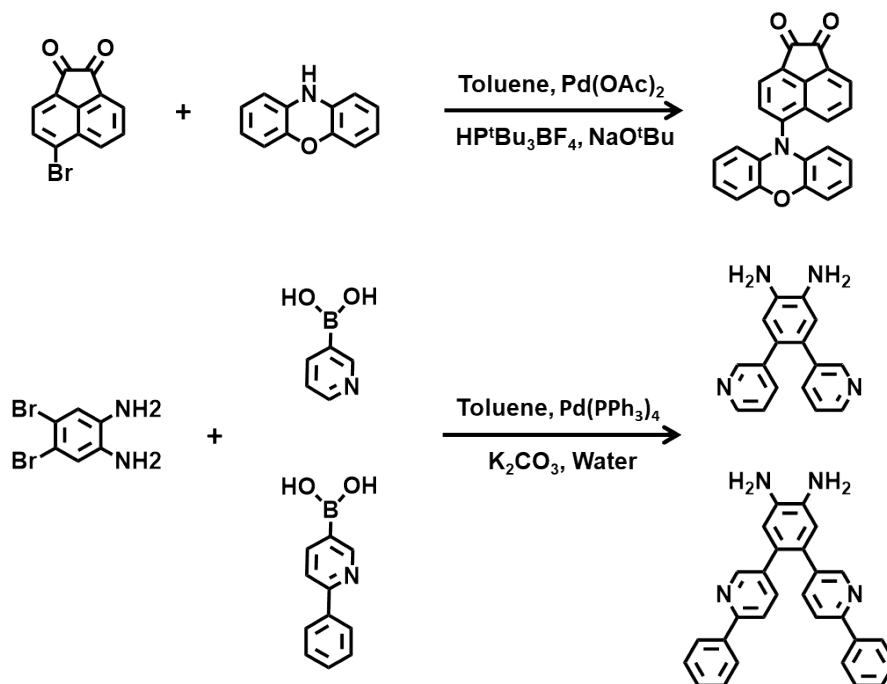
$$k_p = 1/\tau_{PF} \quad (9)$$

$$k_d = 1/\tau_{TADF} \quad (10)$$

Where Φ is the quantum yield of luminescence under nitrogen atmosphere, Φ_{PF} is the quantum yield of prompt fluorescence, Φ_{TADF} is the quantum yield of delayed fluorescence, τ_{PF} is the lifetime of prompt fluorescence, τ_{TADF} is the lifetime of delayed fluorescence, k is the rate constant, and the angle standards p, d, r, nr, ISC and RISC represent the fluorescence, phosphorescence, radiative transition, non-radiative transition, intersystem crossing and reverse intersystem crossing, respectively.

S-II Synthesis

All the reagents and solvents used for the synthesis were purchased from Aldrich or Acros and used as received. All reactions were performed under nitrogen atmosphere. The 5-(10H-phenoxazin-10-yl)acenaphthylene-1,2-dione and (pyridine-3-yl)benzene-1,2-diamine derivatives were synthesized by Buchwald–Hartwig and Suzuki coupling reaction (Scheme 1), respectively, as our previous work.



Scheme 1 Synthetic routes of precursor compounds.

S- III Figures

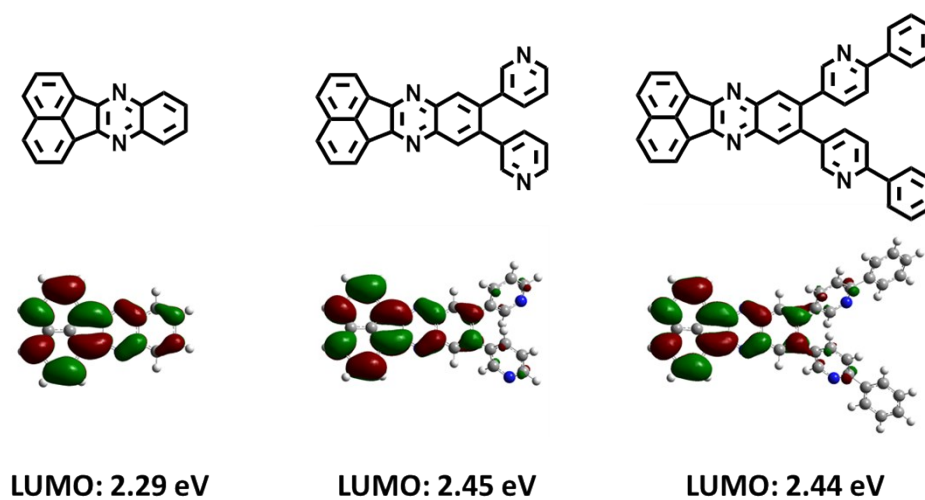


Figure S1. The structures, LUMO distributions and LUMO energy levels of acceptor moieties.

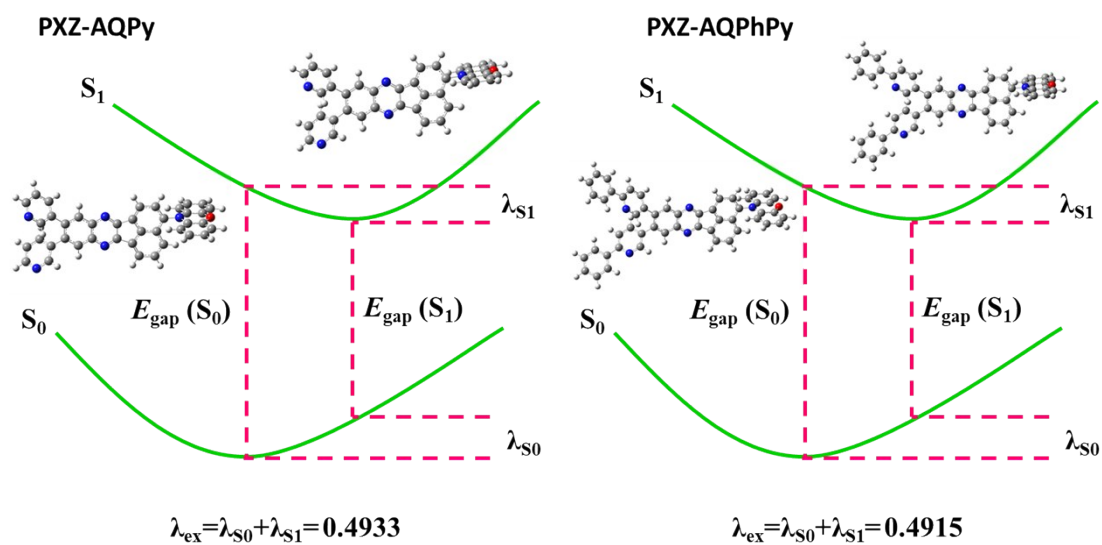


Figure S2. The optimized S_0 , S_1 structures and reorganization energies (λ_{ex}) of PXZ-AQPy and PXZ-AQPhPy.

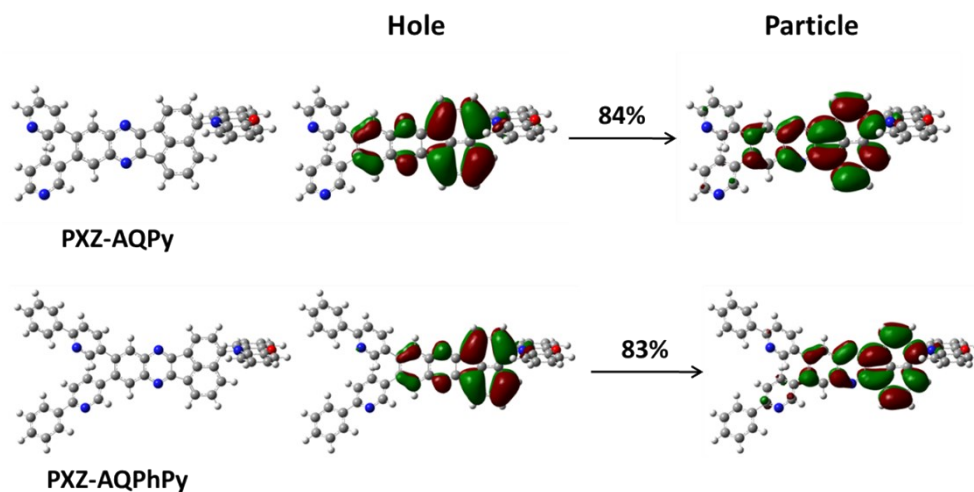


Figure S3. The natural transition orbital (NTO) distributions of T_2 state for PXZ-AQPy and PXZ-AQPhPy.

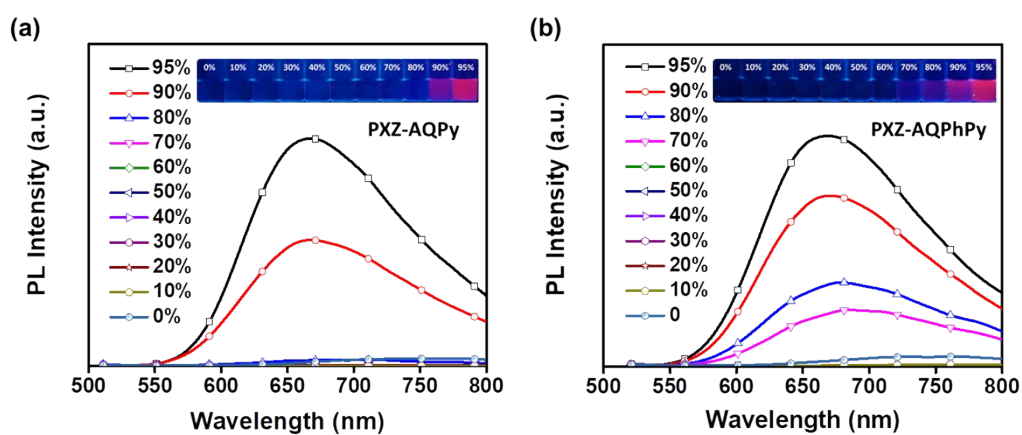


Figure S4. The PL spectra in the mixture of tetrahydrofuran (THF) and water with different water fraction (f_w) of PXZ-AQPy (a) and PXZ-AQPhPy (b).

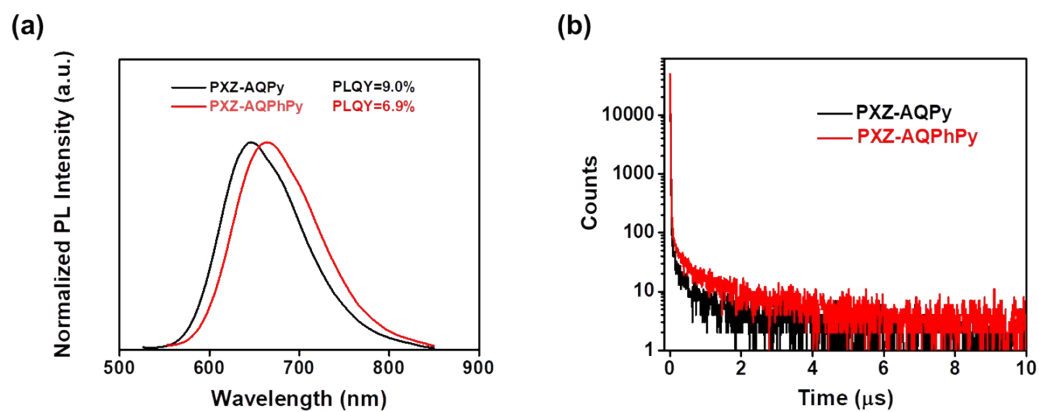


Figure S5. The PL spectra, PLQYs (a) and transient PL spectra (b) of PXZ-AQPy and PXZ-AQPhPy in neat films.

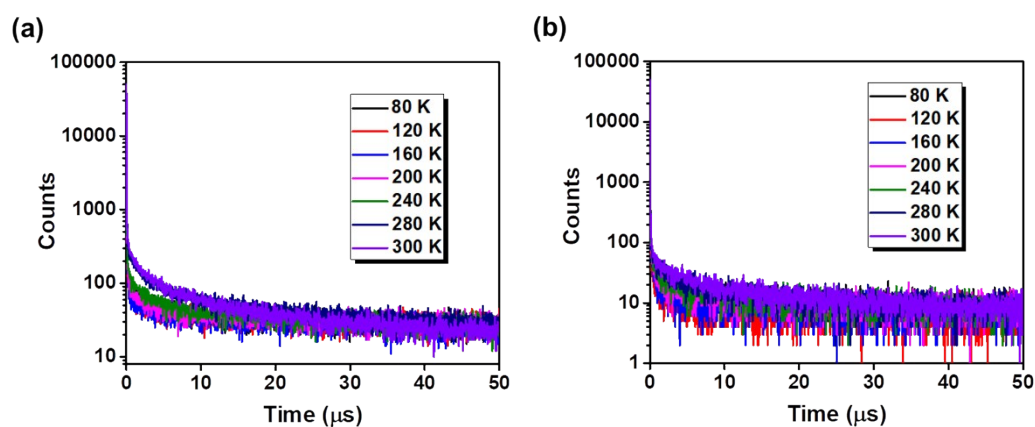


Figure S6. The temperature-dependent transient PL decay spectra of PXZ-AQPy (a) and PXZ-AQPhPy (b).

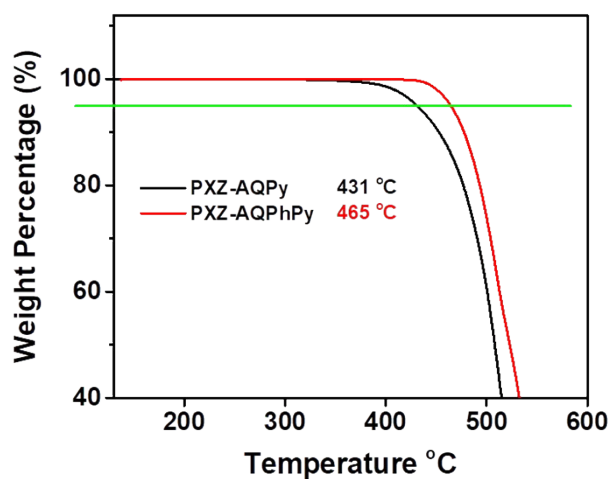


Figure S7. The thermal gravimetric analysis (TGA) curves and thermal degradation temperatures for compounds.